Exploring the N-terminal region of CXCL12: Identification of plasma-stable cyclic peptides as novel, potent CXCR4 antagonists

Salvatore Di Maro,[1] Anna Maria Trotta,[2] Diego Brancaccio,[3,4] Francesco Saverio Di Leva,[3] Valeria La Pietra,[3] Caterina Ieranò,[2] Maria Napolitano,[2] Luigi Portella,[2] Crescenzo D'Alterio,[2] Rosa Anna Siciliano,[5] Deborah Sementa,[3] Stefano Tomassi,[3] Alfonso Carotenuto,[3] Ettore Novellino[3] Stefania Scala[2] and Luciana Marinelli[3*]*

[1]DiSTABiF, Second University of Naples, Via Vivaldi 43, 81100 Caserta, Italy.

[2]Genomica Funzionale. Istituto Nazionale per lo Studio e la Cura dei Tumori, Fondazione "Giovanni Pascale", IRCCS-ITALY, Via M. Semmola 52, 80131 Naples, Italy.

[3]Dipartimento di Farmacia, Università di Napoli "Federico II", via D. Montesano 49, 80131 Naples, Italy.

[4]Laboratory of Food Chemistry, Dipartimento di Agraria (QuaSic.A.Tec.), Università Mediterranea di Reggio Calabria, Reggio Calabria, loc. Feo di Vito, 89122 Reggio Calabria, Italy.

[5]Istituto di Scienze dell'Alimentazione – CNR, Via Roma 64, 83100 Avellino, Italy.

KEYWORDS: CXCR4, CXCL12, CXCR4 antagonists, cancer, molecular invasion, molecular docking, drug design.

Abstract

We previously reported the discovery of a CXCL12-mimetic cyclic peptide (**1**) as selective CXCR4 antagonist showing promising *in vitro* and *in vivo* anticancer activity. However, further development of this peptide was hampered by its degradation in biological fluids as well as by its low micromolar affinity for the receptor. Herein, extensive chemical modifications led to the development of a new analogue (**9**) with enhanced potency, specificity and plasma stability. A combined approach of Ala-amino acid scan, NMR and molecular modeling unraveled the reasons behind the improved binding properties of **9** *vs* **1**. Biological investigations on leukaemia (CEM) and colon (HT-29 and HCT116) cancer cell lines showed that **9** is able to impair CXCL12-mediated cell migration, ERK-phosphorylation and CXCR4 internalization. These outcomes might pave the way for the future preclinical development of **9** in CXCR4 overexpressing leukaemia and colon cancer.

Introduction

Chemokines constitute a family of small cytokines that regulate immunological and inflammatory processes, such as cell chemotaxis, hematopoiesis, and angiogenesis through the interaction with their G protein-coupled receptors (GPCRs).[1] Activation of chemokine receptors by their physiological ligands elicits conformational changes that trigger a signaling cascade involving G protein binding, activation of kinases and Ca^{2+} mobilization from cellular stores, which in turn induce cytoskeletal rearrangement and chemotaxis toward cell attractant molecules.[2,3]

The chemokine CXCL12, a 68-residue polypeptide, also known as stromal cell–derived factor–1 (SDF-1α), belongs to the CXC chemokines subfamily, all featuring two conserved cysteine residues at specific positions in the N-terminal region.[4] CXCL12 is the endogenous ligand of CXCR4, which is one of 19 known human chemokine receptors, and it is primarily coupled with G_i proteins to activate divergent signaling pathways that are involved in multiple important physiological functions such as the development of the hematopoietic, nervous, gastrointestinal and immune systems.[5] In the last decades, CXCL12/CXCR4 axis has been implicated in a wide range of diseases such as infections,[6] inflammations[7] and cancer.[8] Thus, the inhibition of the CXCL12/CXCR4 pathway has emerged as a novel anticancer strategy, widely supported by a large number of in vitro and in vivo studies.[9] In particular, CXCR4 has been shown to play a prognostic role in primary colorectal cancer, alone or in association with the vascular endothelial growth factor (VEGF).[10] In fact, CXCR4 can promote angiogenesis in vitro by modulating the secretion of VEGF.[11,12]

The pursuit of CXCR4 antagonists suitable for anticancer intervention culminated in the identification of plerixafor,[12] previously known as AMD 3100 (1,1'-[1,4-

Phenylenebis(methylene)]bis [1,4,8,11-tetraazacyclotetradecane]). In preclinical models, plerixafor has shown considerable antimetastatic properties, thus, offering the first proof of concept of CXCR4 importance as anticancer target. Plerixafor has been approved from FDA for hematopoietic stem cell mobilization in patients with non-Hodgkin's lymphoma and multiple myeloma undergoing autologous bone marrow transplantation and resistant to conventional protocol for mobilization.[13] Nevertheless, due to poor oral bioavailability and risk of cardiotoxicity, new alternative CXCR4 antagonists have been developed and subjected to preclinical and clinical studies.[14] Among them, AMD 11070 has a reduced basic property compared with Plerixafor and is orally bioavailable. However, it did not achieve maximal pharmacodynamics effect in human based on the elevation of white blood cells [15] Alternatively, some peptide antagonists, such as BKT140[16] and CTCE-9908,[17] also moved to clinical studies, but their application appeared to be partially hampered from *in-vivo in*stability and other pharmacokinetic issues.[16,17] LY2510924,[18] a CXCR4 cyclic antagonist peptide currently engaged in two Phase 2 Studies in Small Cell lung Cancer and Renal Cancer, shows CD34+ cell mobilization at doses ≥ 2.5 mg/day and a tolerable safety profile up to 20 mg/day according to a previous Phase 1 Study. As part of our ongoing efforts in identifying new CXCR4 antagonists, a CXCL12-derived small cyclic peptide (**1**), which selectively interacts with CXCR4, was identified.[19] Although **1** possesses an interesting in vitro and in vivo pharmacological profile, it suffers from degradation in biological fluids (see "Design" paragraph) and its IC_{50} is in the low micromolar range. Herein, to enhance both the CXCR4 affinity and metabolic stability of **1**, we embarked on a lead optimization campaign. By modifying both the N- and C-termini and through a *D*-amino acid scan, a new, potent, selective and serum stable CXCR4 antagonist was identified (**9**). The novel cyclic peptides were assayed against CXCR4 by measuring their ability to inhibit

receptor binding of PE-conjugated-12G5 anti-CXCR4 antibodies and CXCL12 dependent migration in CEM human lymphoblastoid cells, highly expressing CXCR4. Further biological investigations on two different human colon cancer cell lines (HT29 and HCT116) overexpressing CXCR4, confirmed the *in vitro* efficacy and thus the capability to inhibit the CXCR4 receptor as demonstrated through impairment of CXCL12-mediated cell migration and ERK-phosphorylation. A favorable selectivity profile toward CXCR4 over CXCR3 and CXCR7 was also found. Finally, the molecular bases for the improved CXCR4 affinity of **9** were unraveled by NMR and molecular modelling. The improved properties of **9**, with respect to **1**, might pave the way for the future preclinical development of our peptide in CXCR4 overexpressing colon cancer.

Results and Discussion

Design. The peptide (H-Arg-Ala-[Cys-Arg-Phe-Phe-Cys]-COOH) (**1**), previously identified by some of us, inhibits the association between CXCR4 and its ligand CXCL12 at a low micromolar level (IC_{50} = 6.2 μM) and in turn impairs CXCR4 function using *in vitro* and *in vivo* systems.[19] However, as already stated in the "Introduction" paragraph, it displays low stability in biological fluids, as in human serum, **1** starts to be metabolized by 30% after only 30 minutes, and is fully converted into the cyclic pentapeptide cyclo[Cys-Arg-Phe-Phe-Cys] within 2 hours. Interestingly, the inactivation of **1** proceeds through the cleavage of the exocyclic Arg^1-Ala^2 dipeptide at the N-terminal region. Additionally, the IC_{50} of **1** (Table 1), needs to be improved to achieve an optimal *in vivo* activity. Interestingly, from a structural point of view, **1** shares common pharmacophoric features, such as two aromatic and two positively charged residues, with FC131, a cyclic pentapeptide previously described as a potent CXCR4 antagonist.[20] Thus, we envisaged that the micromolar activity of **1** may be ascribable to a wrong orientation of those pharmacophoric amino acids within the receptor binding site. To enhance both the peptide CXCR4 affinity and metabolic stability, a systematic modification scheme was designed. Specifically, to increase the stability of **1**, the N-terminus was acetylated (**2** and **3**, Table 1) while the C-terminus was amidated (**3** and **4**, Table 1). The obtained compounds were validated for inhibiting CXCR4 function through *in vitro* assays evaluating the 12G5 anti-CXCR4 antibody competition and the CXCL12 dependent migration in CEM human lymphoblastoid cells, highly expressing CXCR4. Next, the most promising peptide emerged from this first set of modifications (**2**) was subjected to a *D*-amino acid scan (Table 1, **5-11**) to investigate the role of each residue chirality in the peptide-receptor interaction. A new, stable and potent CXCR4 analogue (**9**) was discovered and the specific

contribution of each putative pharmacophoric side chains was then investigated by performing an *L*-Ala scan (Table 1, **12-15**).

Chemistry. All the peptides were synthesized adopting a classical Fmoc/Boc solid phase peptide strategy. AM-PS resin functionalized with a RINK-amide linker was used for the $CONH_2$-terminal peptides (**3,4,** Table 1), while 2-Cl Clorotrityl resin was selected as solid support for the COOH-terminal peptides (**1,2,5-15,** Table 1) in order to minimize the racemization of the first cysteine residue loaded onto resin.[21] The linear eptapetides were build using standard N-Fmoc/tBu solid-phase peptide synthesis strategy. After the cleavage of the linear eptapeptides from the resin, the resulting free thiol groups were oxidized using Iodine to form a disulfide bridge. The synthetic approach adopted for the generation of the peptides enabled the rapid and efficient synthesis of a small library of peptides.

CXCR4 Binding Assays. The novel cyclic peptides were assayed against CXCR4 measuring their ability to inhibit receptor binding of PE-conjugated-12G5 anti-CXCR4 antibodies in CEM-CCRF human T leukemia CXCR4 expressing cells.[22] As shown in Table 1, the conversion of COOH- into $CONH_2$-termini, in association or not with acetylation of the N-terminus, minimally affected the peptide efficacy. Indeed, **3** and **4** showed IC_{50} of 1.23 and 5.9 μM, respectively. Conversely, **2**, which is the acetyl-derivative of **1**, reduced the association of the 12G5 CXCR4-antibody to the receptor with an IC_{50} of 0.131 μM, resulting to be about 50-fold more potent than the lead (IC_{50} = 6.2 μM). Thus, the N^{α}-acetylation of the Arg^1 residue represented a successful modification only in presence of the COOH-terminus, which appeared to be a critical group for receptor binding. Next, the overall conformation of **2** was modified by performing a *D*-amino acid scan study. The sequential replacement of each residue with its corresponding *D*-isomer resulted in analogues (**5-11**) which mostly had significant weaker binding affinity than **2**, with the lone exception of **9**.

Table 1.Half-maximal inhibitory concentration (IC50, μM, mean ± S.D.) of CXCR4 antagonist peptides necessary to reduce by 50% the binding to CXCR4 of CXCR4-specific mAb 12G5 in CCRF–CEM cells. Each experiment was performed in triplicate

Compound	Sequence	IC_{50} (μM)
1	H-Arg-Ala-[Cys-Arg-Phe-Phe-Cys]-COOH	6.2 ± 1.3
2	**Ac**-Arg-Ala-[Cys-Arg-Phe-Phe-Cys]-COOH	0.131 ± 0.0014
3	**Ac**-Arg-Ala-[Cys-Arg-Phe-Phe-Cys]-**$CONH_2$**	1.23 ± 0.28
4	H-Arg-Ala-[Cys-Arg-Phe-Phe-Cys]-**$CONH_2$**	5.9 ± 0.64
5	Ac-Arg-Ala-[Cys-Arg-Phe-Phe-**DCys**]-COOH	5.9 ± 0.42
6	Ac-Arg-Ala-[Cys-Arg-Phe-**DPhe**-Cys]-COOH	>10
7	Ac-Arg-Ala-[Cys-Arg-**DPhe**-Phe-Cys]-COOH	>10
8	Ac-Arg-Ala-[Cys-**DArg**-Phe-Phe-Cys]-COOH	>10
9	Ac-Arg-Ala-[**DCys**-Arg-Phe-Phe-Cys]-COOH	0.053 ± 0.004
10	Ac-Arg-**DAla**-[Cys-Arg-Phe-Phe-Cys]-COOH	>10
11	Ac-**DArg**-Ala-[Cys-Arg-Phe-Phe-Cys]-COOH	>10
12	Ac-**Ala**-Ala-[DCys-Arg-Phe-Phe-Cys]-COOH	>10
13	Ac-Arg-Ala-[DCys-**Ala**-Phe-Phe-Cys]-COOH	>10
14	Ac-Arg-Ala-[DCys-Arg-**Ala**-Phe-Cys]-COOH	>10
15	Ac-Arg-Ala-[DCys-Arg-Phe-**Ala**-Cys]-COOH	>10
AMD 3100		0.006 ± 0.004

The latter bears a *D*-Cys instead of *L*-Cys at the position 3, and showed an IC_{50} of 0.053 μM, that was 120 times lower than that of **1**. In line with our hypothesis, these data clearly pointed out that the conformational changes induced in **9** through the use of a *D*-amino acid were able to better orientate the pharmacophoric side chains to increase the binding. An alanine-scan study, restricted to the phenylalanine and arginine residues, was then carried out on **9** to assess their role in the peptide binding. As expected, no or very low CXCR4 binding was observed up to 10 μM concentration of the alanine substituted peptides **12-15**.

CXCR3 and CXCR7 Binding Assays. The exclusive binding of a drug to its target is required to avoid potential side effects resulting from the interactions with other receptors. Here, we assessed the selectivity profile of our most potent peptide (**9**) towards other chemokine receptors, specifically CXCR3 and CXCR7. In fact, we evaluated the anti-CXCR3 and anti-CXCR7 efficacy of **9** on a colon cancer cell line (COLO205) overexpressing CXCR3[23] and a breast cancer cell line (MCF-7) overexpressing CXCR7.[24] As shown in Figure 1, **9** did not bind neither CXCR7 nor CXCR3 up to 10 μM concentration. Interestingly, similar results had been previously obtained for **1**,[19] indicating that the chemical modifications here introduced have not affected the selectivity profile of the lead.

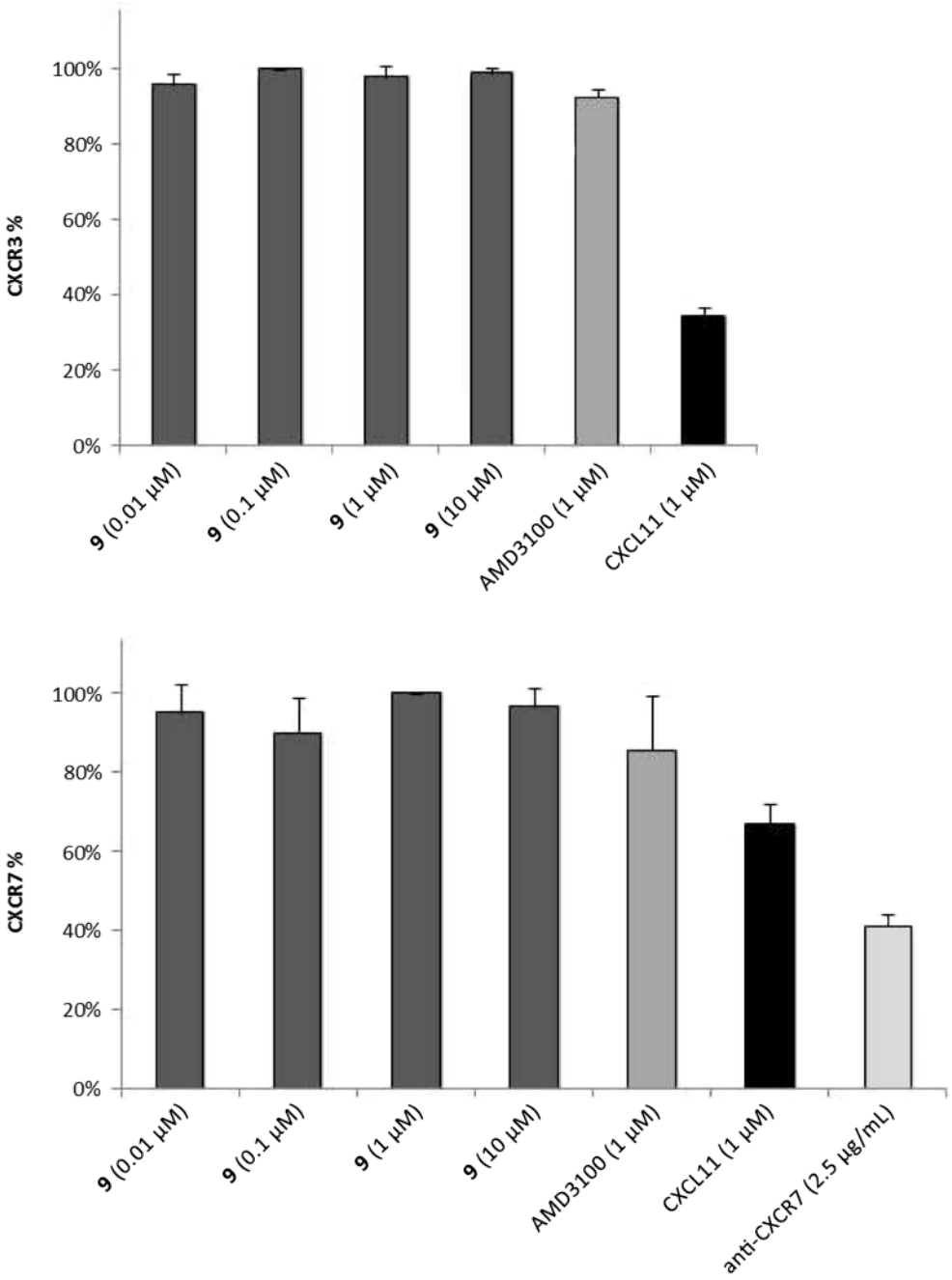

Figure 1. Binding assays on CXCR3 and CXCR7. Indirect binding experiments with the anti-CXCR7, clone 11G8 and anti-CXCR3 clone 49801 were conducted in MCF-7 and COLO205, CXCR7 and CXCR3 overexpressing cells, respectively. Data are presented as bar graph showing mean ± SD.

Cell migration and P-ERK induction experiments. CXCL12 dependent migration and P-ERK induction represent major activities elicited by the CXCL12-induced CXCR4 signaling. For these reasons, we evaluated the ability of the new analogue **9** to inhibit these two CXCR4 functions, in comparison with the parent peptide **1**. CXCL12 dependent migration of CEM cells was evaluated in the presence of **9** or **1**. CEM cells were allowed to migrate toward CXCL12 (100 ng/ml) for 18 hours. As shown in Figure 2 and Figure S2, **9** inhibited CEM migration more efficiently than **1**. The inhibitory dose-dependent effect of 9 on CXCL12 migration in CEM cell (Figure S1) was evaluated, Subsequently, the effect of **1** and **9** on the CXCL12-dependent P-ERK induction (Figure 3) was evaluated, showing that can **9** efficiently inhibit the CXCL12-induced P-ERK more efficiently than **1** (Fig 3a-c).

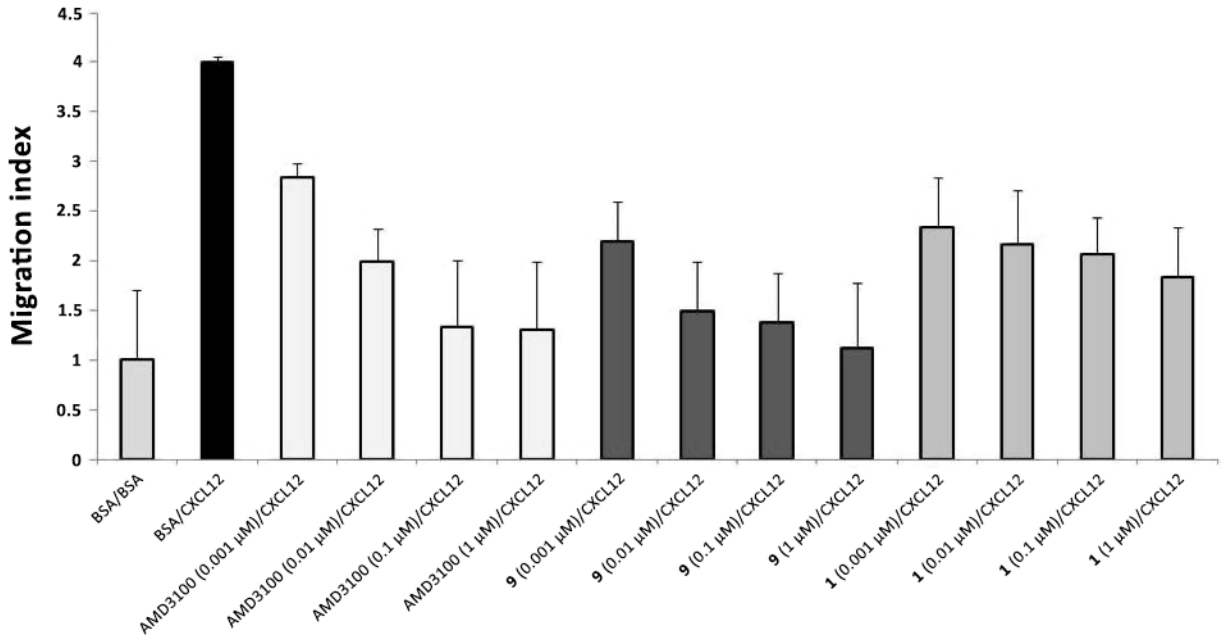

Figure 2. Inhibition of CEM cells migration experiments. Migrated cells on the lower surface were fixed, stained with H&E and counted microscopically. The cells were counted in ten different consecutive high power fields (magnification 400X). The 0.70% of total input cells migrated in buffer alone containing 1% BSA . The results are expressed as migration index (CXCL12 dependent migration/BSA dependent migration). **1** and **9** were compared to the CXCR4 reference antagonist, AMD3100. Data are presented as bar graph showing mean ± S.D.

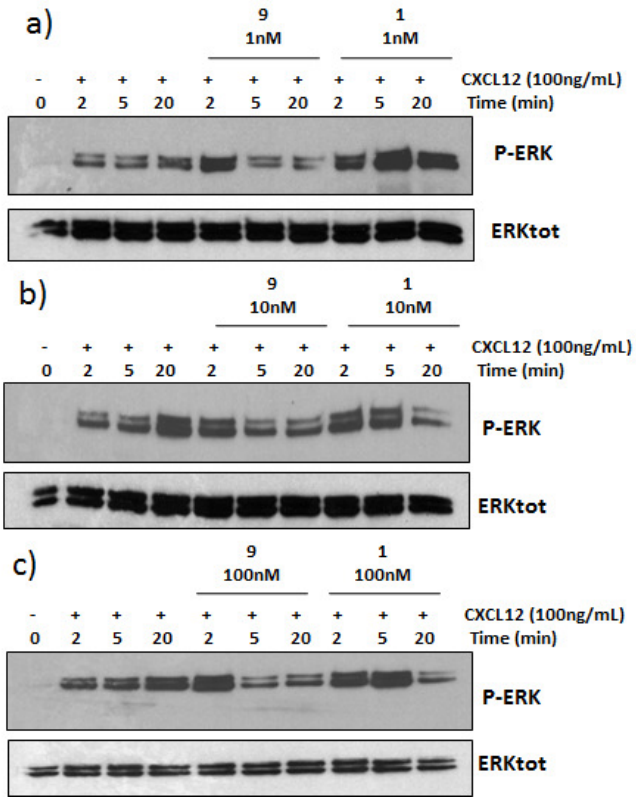

Figure 3. CXCL12-mediated P-ERK induction Assay. CEM cells were serum-starved and treated with CXCL12 (100 ng/ml) in presence of **1** and **9**.

Evaluation of 1 and 9 on Human Colon Cancer Cells. To evaluate the CXCR4 antagonistic activity of **9** in a model suitable for future clinical development, we assessed its efficacy on the CXCR4 overexpressing HT-29 human colon cancer cell line. As shown in Figure 4, in HT-29 cells, **9** binds CXCR4 in a concentration-dependent manner, showing higher potency than **1** (IC_{50} decreased from 5.2 ± 2.6 μM (**1**) to 0.064 ± 0.024 μM (**9**)). Subsequently, the ability of our peptides to inhibit CXCL12 dependent HT-29 cells migration was evaluated. Results of these experiments indicated that both **1** and **9** can affect cells migration towards CXCL12, with the latter being effective even at nanomolar concentration (Figure 4b and Figure S4).

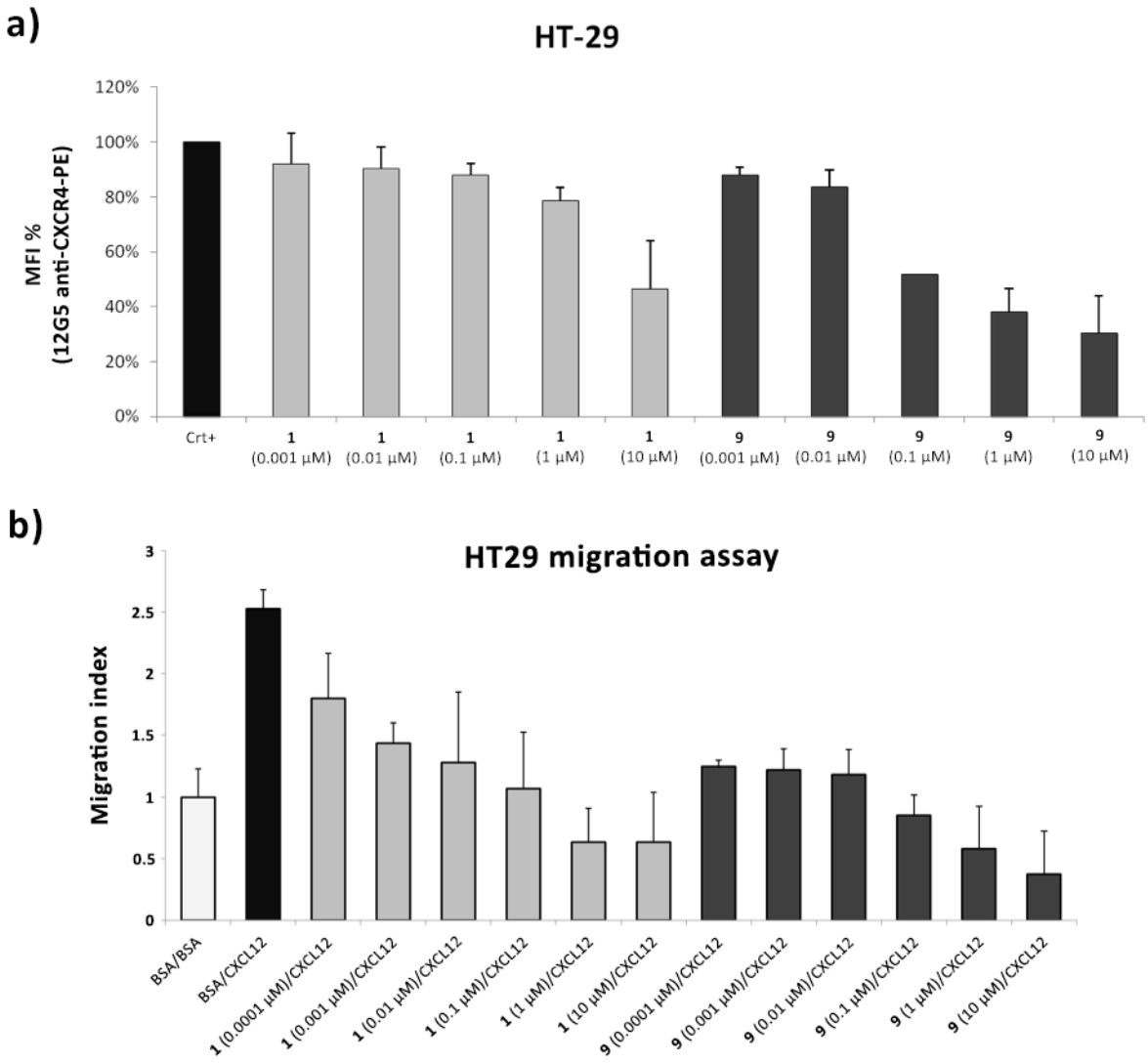

Figure 4. (a) CXCR4 binding experiments on **1** and **9** in human colon cancer cells. CXCR4 binding was indirectly evaluated through inhibition of 12G5 anti-CXCR4 antibody binding in HT29-human colon cancer-CXCR4 expressing cells. (b) CXCL12-induced migration assays on human colon cancer cells HT-29. The 0.81% of total input cells migrated in buffer alone containing 1% BSA.

CXCR4 Internalization Assay. To better understand the effect of **1** and **9** on CXCR4 expression and activation, a receptor internalization assay was carried out on the colon cancer cell line HCT-116 engineered to express human GFP-tagged CXCR4 receptor. HCT-116-GFP-CXCR4 cells were treated with **1** and **9**, then stimulated with 50 ng/ml CXCL12 to induce receptor internalization and observed by confocal microscopy. As showed in Figure 5, in absence of

CXCL12, CXCR4 localizes at both membrane and cytoplasmic level, with some accumulation at the perinuclear region. After 45 min of stimulation with CXCL12, GFP-CXCR4 is extensively internalized as indicated by the reduction of membrane fluorescence intensity and formation of CXCR4 containing intracellular vesicles. In presence of **1** or **9**, receptor internalization is impaired as suggested by intracellular vesicles reduction and consistent membrane fluorescence. A slight further reduction in the vesicles size is detected when the cells were treated with **9** (Figure 5).

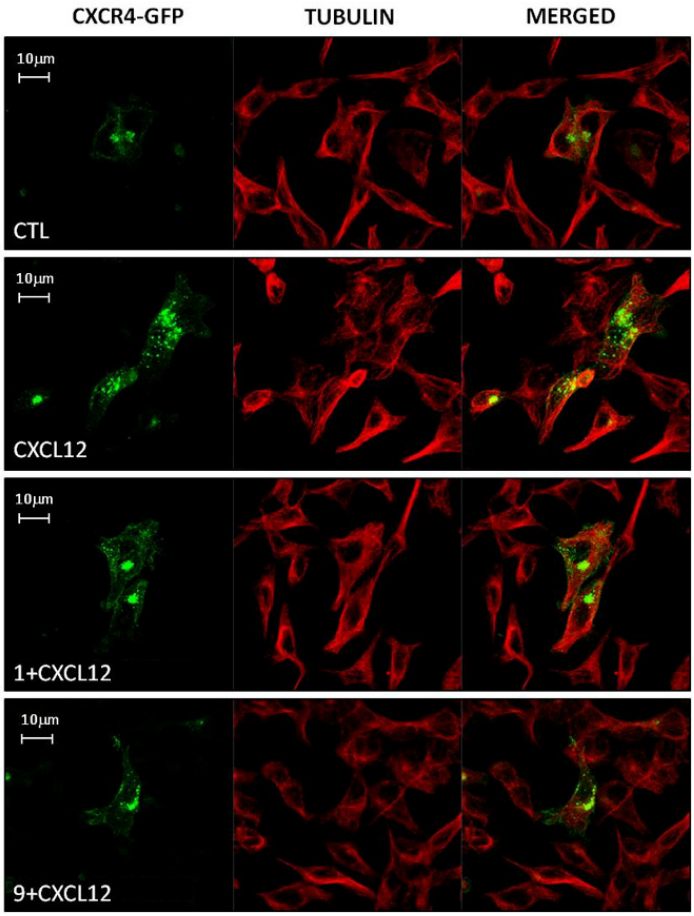

Figure 5: CXCR4 internalization assay. HCT-116 colon cancer cells were engineered to express GFP-tagged CXCR4; α-Tubulin staining were used to define cells cytoplasm and shape. Cells were treated for 45 min with 100 nM of either **1** or **9** and then for 45 min with CXCL12.

Serum Stability Assay. The effects of **1** modifications on metabolic stability were assessed by incubating **1**, **2**, and **9** in diluted human serum at 37 °C adopting a protocol described in literature.[25]

Time course aliquots were collected, treated with acetonitrile to precipitate the plasma proteins and analyzed by ESI-RP-HPLC. As shown in Figure **6**, after 60 min, the concentration of **1** was reduced by 50%, resulting in a cleaved form of the peptide lacking the Arg^1 residue and the Arg^1-Ala^2 dipeptide at the N-terminal region (Fig. 6b). After 120 min, **1** was fully converted into the cyclic pentapeptide metabolite. Conversely, **2** and **9**, both featuring an N-terminal acetyl cap, were stable up to 180 min. Taken together, these results clearly pointed out that the acetyl group at the N-terminal region was sufficient to protect the peptide against human serum proteolytic degradation.

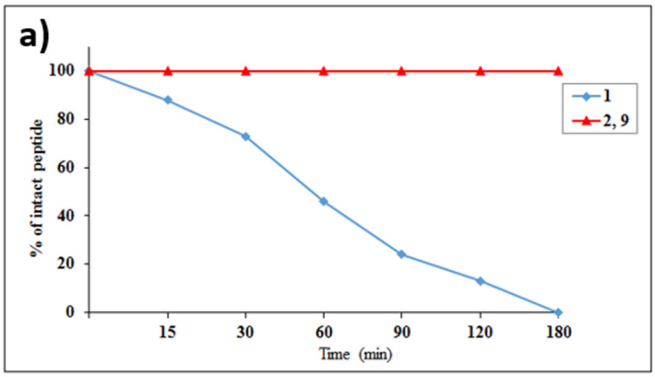

b)

Compound	aa sequence	m/z[a]					
		0 min	15 min	30 min	60 min	120 min	180 min
1	RA[CRFFC]	900.4	900.4[b]	900.4	900.4	900.4	
			788.3[c]	788.3	788.3	788.3	788.3
			673.3[d]	673.3	673.3	673.3	673.3
2	Ac-RA[CRFFC]	942.5	942.5	942.5	942.5	942.5	942.5
9	Ac-RA[cRFFC]	942.5	942.5	942.5	942.5	942.5	942.5

[a] Found ESI-MS, $[M+H]^+$,

[b] 1

[c] 1-R

[d] 1-RA

Figure 6. (a) Human serum stability profiles of **1** and **9** after different intervals of incubation with human serum. Relative concentrations of peptides were determined by integration of the A230 peaks from RP-HPLC (b) ESI-MS characterizations of **1** and **9** at different intervals of incubation.

NMR Spectroscopy. NMR experiments were performed on **1** and **9** in order to understand the conformational differences induced in our peptides by the diverse configuration of the Cys^3 residue

and by the introduction of an acetyl N-cap. Complete ^{1}H NMR chemical shift assignments (Table S1 and S2) were performed for **1** and **9** according to the Wüthrich[26] procedure. DQF-COSY,[27] TOCSY,[28] and NOESY[29] experiments, with the support of the XEASY software package[30] were carried out in 200 mM SDS micellar solution. The employment of SDS micelles to investigate the conformational properties is justified on the basis of their interaction with a membrane receptor. For peptides that bind membrane receptors, such as GPCR, the use of membrane mimetic solution is suggested, assuming a membrane-assisted mechanism of interactions between the peptides and their receptors,[31] hence micelle solutions have been extensively used for peptide hormones conformational studies.[32] For both peptides, NMR parameters indicated the presence of β-turn structures. In particular, NOE contacts between H_{α}-NH_{i+2} of Arg^{1} and *D*-Cys^{3} and Arg^{4} and Phe^{6} suggested turn structures encompassing residues 1-3 and 3-6, respectively. The presence of turn structures is confirmed by low values of temperature coefficients of amide protons ($|\Delta\delta/\Delta T|<4$ ppb/K) of Phe^{5} and Phe^{6} for both peptides and *D*-Cys^{3} for **9** (Table S1 and S2). Upfield shifts of side chain protons of the Arg^{4} and Phe^{5} residues, and NOE contacts between Arg^{4} and Phe^{5} and between Phe^{5} and Phe^{6} point to a spatial proximity of these couple of side chains in both peptides. For both peptides, NMR constraints from SDS micelle solution were used as the input data for a simulated annealing structure calculation. Two ensembles of well-defined structures were obtained. In fact, the 10 lowest energy structures for **1** (Figure 7a) and **9** (Figure 7b), showed a backbone RMSD of 0.19 and 0.17 Å, respectively, that satisfied the NMR-derived constraints (violations smaller than 0.40 Å). Predicted turn structures were found in both peptides: a γ-turn along residues 1-3 and a type IV β-turn along residues 3-6. Interestingly, in **1** calculated structures, Cys^{3} shows a positive value of the dihedral angle φ (~60°) which could explain the observed constructive replacement with a *D*-Cys residue. The main difference between the two peptide

structures consists in the different spatial disposition of the Arg[1] side chain which is close to Phe[5] and Phe[6] only in **9** as confirmed by various NOE interactions between Arg[1] with Phe[5], and acetyl protons with Phe[6] observable only in the NOESY spectrum of **9** while missing in that of **1**. Geometry of *D*-Cys residue and lipophilicity of the acetyl moiety in **9** must be responsible for the observed difference. Interestingly, Ala- and *D*-scan results clearly demonstrated that both functionality and spatial arrangement of Arg[1] side chain matter for the activity of our derivatives. Hence, Arg[1] side chain reorientation in **9** is likely to contribute to the increased potency of the peptide. This issue has been further investigated by molecular modeling studies.

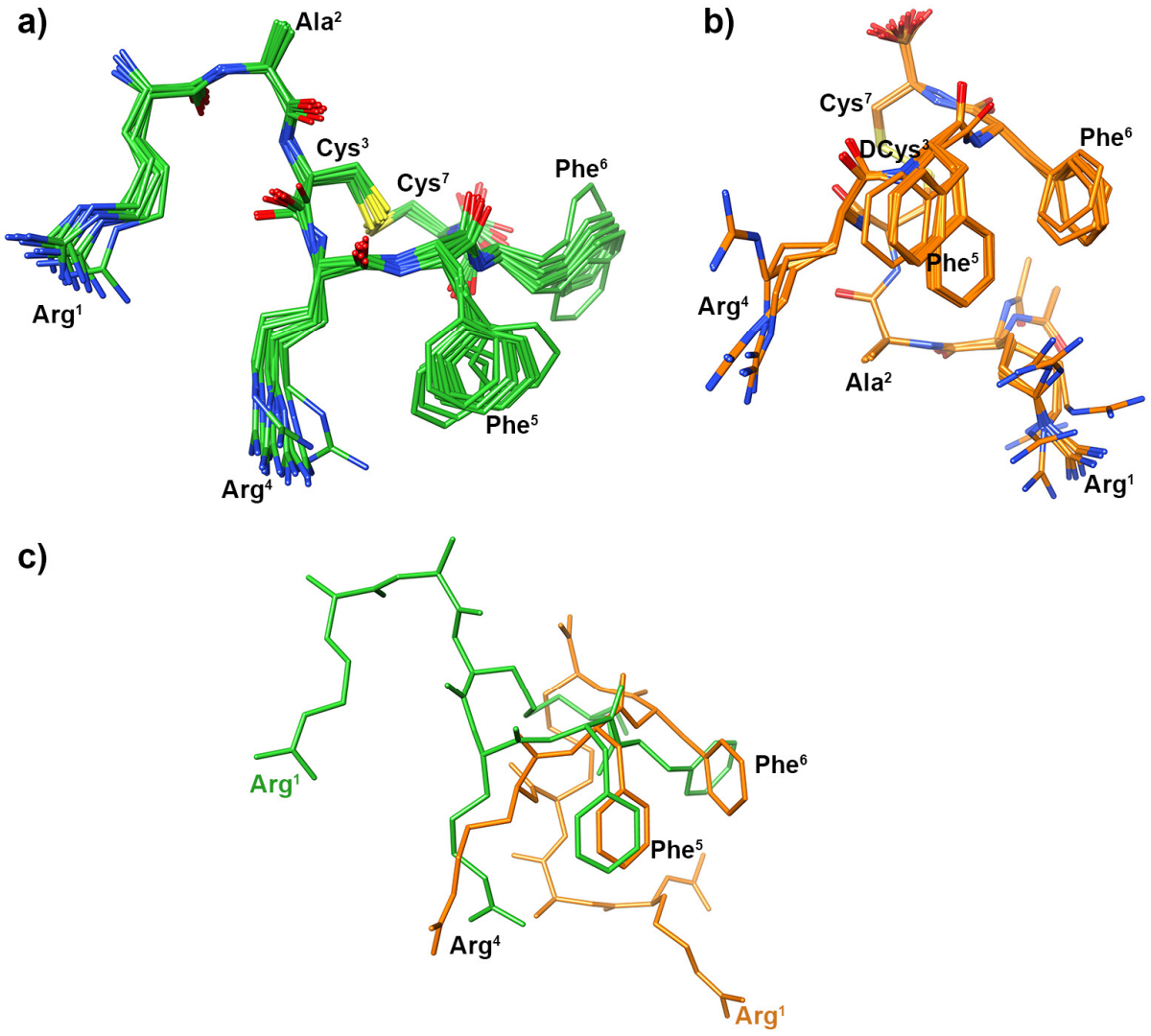

Figure 7. Superposition of the ten lowest energy conformers of **1** (a) and **9** (b). Structure models were superimposed using the backbone heavy atoms. Heavy atoms have different colors (carbon: orange/green, nitrogen: blue, oxygen: red, sulfur: yellow). Hydrogen atoms are hidden for clarity reasons. (c) Superposition of **1** (green) with **9** (orange) using the three main pharmacophoric points: the guanidino group of the Arg^4 and the centroids of both the Phe^5 and Phe^6 phenyl rings.

Molecular Modeling. To investigate at an atomic level the binding to CXCR4 of the most potent peptide of the series, namely **9**, extensive computational studies were performed. In the present case, straightforward docking methods did not represent the best option, as they cannot thoroughly sample the large conformational space of mid-high molecular weight peptides upon binding. For this reason, and to take into account the receptor flexibility and the biological environment, we performed an over 100 ns molecular dynamics (MD) simulation on the **9**/CXCR4 complex in explicit solvent and membrane. The starting binding conformation was obtained through a manual docking of **9** in the crystal structure of CXCR4 in complex with the 16-mer cyclic peptide CVX15 (PDB code 3OE0). Specifically, a superposition between **9** and CVX15 was accomplished based on previous structure–activity relationship (SAR) studies on potent CXCR4 peptide antagonists, which share one positively charged and two aromatic side chains as common pharmacophoric features.[33] (see Experimental Section for details).

At the very beginning of the MD calculations, **9** slightly rearranges at the CXCR4 binding site, assuming a conformation that is almost conserved for the rest of the simulation (Figure S3). In this position (Figure 8), the peptide Arg^1 and Arg^4 side chains make tight salt bridges with the D187 and D97 carboxylate groups, respectively, whereas the Phe^5 and Phe^6 side chains are buried into a semi-aromatic pocket where they can establish favorable interactions with the side chains of Y116,

L120, R188, F199, H203, Y255, and I259. Additionally, water-mediated hydrogen bonds are formed between the Arg^{1} and N37 side chains, and between the Phe^{6} backbone amide and the E288 carboxylate moiety. Interestingly, a number of intra-molecular interactions can be also observed, which are likely to stabilize the peptide bioactive conformation. In particular, the Arg^{1} side chain is hydrogen bonded to the Cys^{7} terminal carboxylate and to the N-acetyl carbonyl group, while an additional H-bond is established between the *D*-Cys^{3} CO and the Cys^{7} NH groups. Overall, this interaction pattern is consistent with the low nanomolar IC_{50} of **9** and in agreement with mutagenesis data reporting residues such D97, H113, Y116, D187 and E288 as critical for ligand binding to CXCR4.[33,34] Furthermore, comparative studies on **1** (see the Supporting Information for details) helped us to elucidate the molecular bases for the improved CXCR4 binding affinity of **9** with respect to the lead peptide. In fact, some differences can be observed in the binding mode of the two peptides, which are ascribable to the inverted chirality of the Cys^{3} residue and the absence of the N-acetyl cap in **1** (Figure S4). For instance, differently from **9**, the Arg^{1} side chain of **1** cannot contact D187 side chain but extends out of the binding site where it might interact with the lipids polar heads. Moreover, the intra-molecular H-bonds formerly described for **9** (i.e. between the Arg^{1} side chain and the Cys^{7} terminal carboxylate) are not observed in the case of **1**, turning out in a lower conformation stability that might negatively impact the binding.

The here presented interaction models also allow rationalizing the effects of all the introduced chemical modifications on our peptides potency. In particular, i) mutation into Ala of Arg^{1}, Arg^{4}, Phe^{5} and Phe^{6} (**12**-**15**) is detrimental for peptide affinity towards CXCR4 since the side chains of these residues represent the major anchor points for receptor binding; ii) the chiralities of the amino acids occupying positions from 3 to 7 (**5**-**11**), particularly *D*-Cys^{3} and Cys^{7}, are crucial to stabilize the binding of the peptide pharmacophoric groups at the CXCR4 receptor; iii) amidation of the

Cys^{7} terminal carboxylate and/or removal of the N-Ac cap (**1**-**4**) lower the peptide affinity towards CXCR4 since such groups participate in intra-molecular interactions that contribute to stabilize the peptide binding conformation. Finally, our model suggests that at least one of the two Phe residues in **9** might be substituted with bulkier aromatic residues, such as 1- or 2-Nal, providing some hints for a further optimization of our peptides potency.

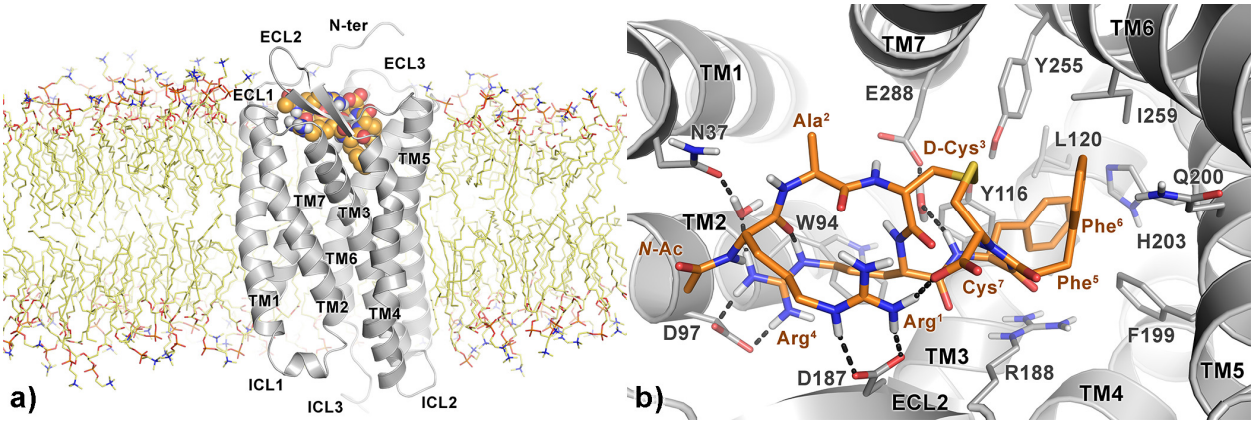

Figure 8. (a) Side view of the predicted CXCR4/**9** complex embedded in the POPC bilayer. CXCR4 is represented as grey cartoons, while the peptide is shown as orange spheres. Lipids are shown as yellow sticks. (b) Binding mode of **9** (orange sticks) at the CXCR4 receptor (grey cartoons) obtained through over 100 ns long MD simulations. Receptor amino acids and waters important for peptide binding are shown as sticks. Hydrogen-bonds are displayed as dashed black lines. Nonpolar hydrogens are omitted for clarity reasons.

Conclusion

In recent years, the CXCL12/CXCR4 pathway has emerged as a major target for the therapy of multiple diseases including various types of blood and solid tumors. For this reason, a number of CXCR4 antagonists are now used or are entering as diagnostic and therapeutic tools for cancer treatment. However, in spite of the medicinal chemists' efforts, the majority of the available CXCR4 antagonists suffer pharmacokinetic or toxicity issues, prompting the design of new anti-CXCR4 ligands with improved pharmacological properties. In this scenario, some of us recently developed a CXCL12-derived cyclic peptide as selective CXCR4 antagonist (**1**). Herein, through a rational lead optimization strategy, we improved both, the binding potency which was in the low micromolar range, and the metabolic stability of **1** affording a nanomolar, selective and plasma stable CXCR4 antagonist (**9**). Ala-amino acid scan, extensive NMR and computational studies elucidated the binding mode of **9** to CXCR4, providing reasons for the increased binding with respect to **1**. In parallel, cell-based assays revealed that **9** inhibits, at nanomolar concentration, both the CXCL12-induced migration and ERK phosphorilation, which are hallmarks for monitoring CXCR4 functions. Finally, we were able to demonstrate that **9** impairs CXCR4 internalization in human colon cancer cells overexpressing CXCR4, which might lay the foundations for a future preclinical investigation of our novel peptide.

Experimental Section

Chemistry

Materials. N^{α}-Fmoc-protected amino acids, 2-Cl-trtCl resin, Fmoc-Rink Amide-Am resin, O-benzotriazole-N,N,N′,N′-tetramethyl-uroniumhexafluorophosphate (HBTU), N,N-diisopropylethylamine (DIEA), triisopropylsilane (TIS), trifluoroacetic acid (TFA), and piperidine were purchased from IRIS Biotech, N-hydroxybenzotriazole (HOBt), N,N-dimethylformamide (DMF), dichloromethane (DCM), and from Iris-Biotech Gmbh (Marktredwitz, Germany). Peptide synthesis solvents, reagents, H_2O and CH_3CN for HPLC were reagent grade and were acquired from commercial sources (Sigma-Aldrich, Milano, Italy) and used as received unless otherwise noted. Peptides were purified by preparative HPLC (Shimadzu HPLC system) equipped with a C18-bounded preparative RP-HPLC column (Phenomenex Kinetex 21.2 mm × 150 mm 5 μm). Peptides were analyzed by analytical HPLC (Shimadzu Prominance HPLC system) equipped with a C18-bounded analytical RP-HPLC column (Phenomenex Kinetex, 4.6 mm × 250 mm 5 μM) using a gradient elution (10–90% acetonitrile in water (0.1% TFA) over 15 min; flow rate = 1.0 mL/min; diode array UV detector). Molecular weights of compounds were confirmed by ESI-mass spectrometry using an Agilent 6110 quadrupole LC/MS system.

General Procedure for COOH-Terminal Peptides. 2-Cl-trtCl resin (62.0 mg, 1.60 mmol/g) was swollen in DCM over 0.5 h, and a solution of Fmoc-*L*-Cys(trt)-OH (87.9 mg, 0.15 mmol, 1.5 equiv) and DIPEA (26 μl, 1.5eq) in DCM (2ml) was added. The mixture was stirred for 10 min. An additional amount of DIPEA (34.8 μl, 0.2 mmol, 2 equiv) was added and the mixture was then shaken for 1 h. The residual chloride groups contained in the resin were capped by adding MeOH (200 μl) in DCM (2 ml) and stirring for 15 min to avoid eventually parallel synthesis of side products. Fmoc group removal was performed using 20 % piperidine in DMF (1 x 5 min and 1 x

25 min). The peptide resin was then washed with DCM (3 x 0.5 min) and DMF (3 x 0.5 min) and positive Kaiser ninhydrine[35] and TNBS[36] tests were observed. Fmoc-*L*-Phe-OH (155.0 mg, 0.4 mmol, 4 equiv) or Fmoc-*D*-Phe-OH (155.0 mg, 0.4 mmol, 4 equiv) or Fmoc-*L*-Ala-OH (124.5 mg, 0.4 mmol, 4 equiv), Fmoc-*L*-Arg(Pbf)-OH (259. 5 mg, 0.4mmol, 4 equiv) or Fmoc-*D*-Arg(Pbf)-OH (259. 5 mg, 0.4 mmol, 4 equiv) or Fmoc-*L*-Ala-OH (124.5 mg, 0.4 mmol, 4 equiv) , Fmoc-*L*-Cys(Trt)-OH (234.3 mg, 0.4 mmol, 4 equiv) or Fmoc-*D*-Cys(Trt)-OH (234.3 mg, 0.4 mmol, 4 equiv), Fmoc-*L*-Ala-OH (124.5 mg, 0.4 mmoli, 4 equiv) or Fmoc-*D*-Ala-OH (124.5 mg, 0.4 mmol, 4 equiv) were sequentially added sequentially to the resin bound H-*L*-Cys(Trt). Each coupling reaction was achieved using a 4-fold excess of amino acid with HBTU (151. 7 mg, 0.4 mmol, 4 equiv) and HOBt (61.2 mg, 0.4 mmol, 4 equiv) in the presence of DIPEA (140 µl, 0.8 mmol, 8 equiv) in DMF. Fmoc deprotections were accomplished with 20% piperidine in DMF solution (1 x 5 min, 1 x 25 min). Washings with DMF (3 x 0.5 min) and DCM (3 x 0.5 min) were performed through every coupling/deprotection step. Kaiser ninhydrine and TNBS tests were employed for monitoring the progress of peptide synthesis. For the peptides bearing an acetyl group at the N-terminus, after removing the last Fmoc group, the resin bound peptide was treated with Ac_2O (19 µl, 0.2 mmol, 2 equiv) and DIPEA (35 µl, 0.2 mmol, 2 equiv) in DCM (2 ml) and the mixture was shaken for 1 h. A negative Kaiser ninhydrine and TNBS tests were observed.

General Procedure for $CONH_2$-Terminal Peptides. Rink amide resin (208 mg, 0.48 mmol/g) was swollen in DMF over 0.5 h and the Fmoc protecting group of the linker was removed with 20 % piperidine in DMF solution (1 x 5 min and 1 x 25 min). The resin was washed with DMF (3 x 0.5 min) and DCM (3 x 0.5 min) and positive Kaiser Ninhydrine and TNBS tests were observed. The linear sequences were assembled sequentially adding Fmoc-*L*-Cys(trt)-OH (234.3 mg, 0.4 mmoli, 4 equiv), Fmoc-*L*-Phe-OH (154.98 mg, 0.4 mmol, 4 equiv), Fmoc-*L*-Arg(Pbf)-OH (259.

51 mg, 0.4 mmol, 4 equiv), Fmoc-*L*-Cys(trt)-OH (234.3mg, 0.4 mmol, 4 equiv), Fmoc-*L*-Ala-OH (124.54 mg, 0.4 mmol, 4 equiv).

Each coupling reaction was achieved using a 4-fold excess of amino acid in presence of HBTU (151.7 mg, 0.4 mmol, 4 equiv)HOBt (61.2 mg, 0.4 mmoli, 4 equiv), and DIPEA (140 µl, 0.8 mmoli, 8 equiv) in DMF (3 ml).. Fmoc deprotections were accomplished with 20% piperidine solution in DMF (1 x 5 min, 1 x 25 min). Washings with DMF (3 x 0.5 min) and DCM (3 x 0.5 min) were performed through every coupling/deprotection step. Kaiser ninhydrine and TNBS tests were employed for monitoring the progress of peptide synthesis. For the peptides bearing an acetyl group at the N-terminus, after removing the last Fmoc group, the resin bound peptide was treated with Ac_2O (19 µl, 0.2 mmol, 2 equiv) and DIPEA (35 µl, 0.2 mmol, 2 equiv) in DCM (2 ml) and the mixture was shaken for 1 h. A negative Kaiser ninhydrine and TNBS tests were observed.

General Procedure for Peptide Oxidation and Purification. The peptide was released from the solid support and all the protecting groups cleaved, treating the resin with TFA/DCM/TIS (80/15/5, v/v/v) (3 ml solvent/0.1 mmol) for 2 h. The resin was then filtered off and the crude linear peptide was recovered by precipitation with chilled ether to give a powder. The crude peptide (0.1 mmol) was dissolved in 30 ml of glacial AcOH and 200 µl of HCl 1N were added to improve the solubility of the peptide. Next, a solution of Iodine (40 mg, mmol) in glacial AcOH (5 ml) was added and the mixture was mechanical stirring for 12 h at room temperature. The resulting mixture was concentrated in vacuo by rotatory evaporator (1/4 of the original volume), transferred to a 50 ml conical centrifuge tube, where the oxydated crude peptide was precipitated by adding 40 ml of chilled ether, recovered by filtration and dried overnight. Final peptide purification was achieved by preparative RP-HPLC in 0.1% TFA with an ACN gradient (10–90% ACN in H_2O over 15 min, flow rate of 15 mL/min) on a Phenomenex Kinetex C18 column (21.2 mm × 150 mm 5 µm).

Analytical RP-HPLC were performed in 0.1% TFA with an ACN gradient (10–90% ACN in H_2O over 20 min, flow rate of 1.0 mL/min) on a Phenomenex Kinetex C18 column (0.46 mm × 150 mm 5 μm).

1. Purity > 95%, t_R 12.2 min (analytical HPLC, 10–90% ACN in H_2O (0.1% TFA) over 15 min, flow rate of 1.0 mL/min); molecular formula: $C_{39}H_{57}N_{13}O_8S_2$; calculated mass: 899.4; found: 900.3 ($M+H^+$), 450.7 ($M+2H^+$)/2.

2. Purity > 95%, t_R 12.5 min (analytical HPLC, 10–90% ACN in H_2O (0.1% TFA) over 15 min, flow rate of 1.0 mL/min); molecular formula: $C_{41}H_{59}N_{13}O_9S_2$; calculated mass: 941.4; found: 942.6 ($M+H^+$), 471.4 ($M+2H^+$)/2.

3. Purity > 95%, t_R 12.0 min (analytical HPLC, 10–90% ACN in H_2O (0.1% TFA) over 15 min, flow rate of 1.0 mL/min); molecular formula: $C_{39}H_{57}N_{13}O_8S_2$; calculated mass: 898.4; found: 899.6 ($M+H^+$), 450.0 ($M+2H^+$)/2.

4. Purity > 95%, t_R 12.2 min (analytical HPLC, 10–90% ACN in H_2O (0.1% TFA) over 15 min, flow rate of 1.0 mL/min); molecular formula: $C_{41}H_{60}N_{14}O_8S_2$; calculated mass: 940.4; found: 941.6 ($M+H^+$), 471.0 ($M+2H^+$)/2.

5. Purity > 95%, t_R 12.6 min (analytical HPLC, 10–90% ACN in H_2O (0.1% TFA) over 15 min, flow rate of 1.0 mL/min); molecular formula: $C_{41}H_{59}N_{13}O_9S_2$; calculated mass: 941.4; found: 942.5 ($M+H^+$), 471.8 ($M+2H^+$)/2.

6. Purity > 95%, t_R 12.6 min (analytical HPLC, 10–90% ACN in H_2O (0.1% TFA) over 15 min, flow rate of 1.0 mL/min); molecular formula: $C_{41}H_{59}N_{13}O_9S_2$; calculated mass: 941.4; found: 942.4 ($M+H^+$), 471.8 ($M+2H^+$)/2, 964.5 ($M+Na^+$).

7. Purity > 95%, t_R 12.4 min (analytical HPLC, 10–90% ACN in H_2O (0.1% TFA) over 15 min, flow rate of 1.0 mL/min); molecular formula: $C_{41}H_{59}N_{13}O_9S_2$; calculated mass: 941.4; found: 942.4 ($M+H^+$), 471.8 ($M+2H^+$)/2.

8. Purity > 95%, t_R 12.4 min (analytical HPLC, 10–90% ACN in H_2O (0.1% TFA) over 15 min, flow rate of 1.0 mL/min); molecular formula: $C_{41}H_{59}N_{13}O_9S_2$; calculated mass: 941.4; found: 942.4 ($M+H^+$), 471.8 ($M+2H^+$)/2.

9. Purity > 95%, t_R 12.6 min (analytical HPLC, 10–90% ACN in H_2O (0.1% TFA) over 15 min, flow rate of 1.0 mL/min); molecular formula: $C_{41}H_{59}N_{13}O_9S_2$; calculated mass: 941.4; found: 942.4 ($M+H^+$), 471.8 ($M+2H^+$)/2, 964.4 ($M+Na^+$).

10. Purity > 95%, t_R 12.5 min (analytical HPLC, 10–90% ACN in H_2O (0.1% TFA) over 15 min, flow rate of 1.0 mL/min); molecular formula: $C_{41}H_{59}N_{13}O_9S_2$; calculated mass: 941.4; found: 942.4 ($M+H^+$), 471.8 ($M+2H^+$)/2.

11. Purity > 95%, t_R 12.5 min (analytical HPLC, 10–90% ACN in H_2O (0.1% TFA) over 15 min, flow rate of 1.0 mL/min); molecular formula: $C_{41}H_{59}N_{13}O_9S_2$; calculated mass: 941.4; found: 942.6 ($M+H^+$), 471.8 ($M+2H^+$)/2, 964.5 ($M+Na^+$).

12. Purity > 95%, t_R 15.1 min (analytical HPLC, 10–90% ACN in H_2O (0.1% TFA) over 15 min, flow rate of 1.0 mL/min); molecular formula: $C_{38}H_{52}N_{10}O_9S_2$; calculated mass: 856.3; found: 857.4 ($M+H^+$).

13. Purity > 95%, t_R 15.1 min (analytical HPLC, 10–90% ACN in H_2O (0.1% TFA) over 15 min, flow rate of 1.0 mL/min); molecular formula: $C_{38}H_{52}N_{10}O_9S_2$; calculated mass: 856.3; found: 857.4 ($M+H^+$).

14. Purity > 95%, t_R 13.6 min (analytical HPLC, 10–90% ACN in H_2O (0.1% TFA) over 15 min, flow rate of 1.0 mL/min); molecular formula: $C_{35}H_{55}N_{13}O_9S_2$; calculated mass: 865.4; found: 866.4 ($M+H^+$), 433.7 ($M+2H^+$).

15. Purity > 95%, t_R 13.8 min (analytical HPLC, 10–90% ACN in H_2O (0.1% TFA) over 15 min, flow rate of 1.0 mL/min); molecular formula: $C_{35}H_{55}N_{13}O_9S_2$; calculated mass: 865.4; found: 866.4 ($M+H^+$), 433.7 ($M+2H^+$).

Human Plasma Stability Assay. Human plasma, H_2O, ACN and TFA were obtained from Sigma-Aldrich (Milano, Italy) and used without further purification. Analytical HPLC-ESI-MS was performed on an Agilent Technologies 1200 Series equipped with an Agilent Technologies 6110 Quadrupole LC/MS using a Phenomenex Luna C18 column (5 μm, 4.6 × 150 mm) and H_2O (0.1% *v*/*v* TFA) / ACN (0.1% *v*/*v* TFA) as eluents.

A solution of 1 mg/ml of each peptide was prepared in water, and 150 μl aliquots were mixed with 150 μl of pre-warmed (37°C) plasma. At selected time points (0, 30, 60, 120 and 180 min), samples (50 μl) were collected and mixed with 1% TFA in acetonitrile (75 μl) to precipitate plasma proteins which were deleted by centrifugation at 13,000 rpm for 10 minutes. The supernatant was analysed by HPLC-ESI-MS (Figure S2, S3, S4 and Table S4) using a Phenomenex Luna C18 column (5 μm, 4.6 × 150 mm) and an elution gradient of 10% - 90% solvent B over 20 min (Solvent A: 0.1% TFA in water; solvent B: 0.1% TFA ACN) at a flow rate of 1 ml/min.

Biological Studies

Binding Assay. CXCR4 binding was evaluated as previously described.[22] Briefly, 5×10^5 CCRF–CEM, HT29 cells were pre-incubated with increasing peptide concentrations (0.01 μM, 0.1 μM, 1 μM, 10 μM) in the binding buffer (PBS 1x plus 0.2% BSA and 0.1% NaN3) for 30 minutes at

37° C, 5% CO_2 and then labeled for 30 minutes using anti-CXCR4 PE-antibody (FAB170P, clone 12G5, R&D Systems, Minneapolis, MN, USA). To evaluate the specific peptide binding to CXCR4, the experiments were also conducted in COLO205, human colon cancer cells, overexpressing CXCR3, using anti-CXCR3 FITC-antibody (R&D FAB160F clone 49801) and in MCF-7, human breast cancer cell line, overexpressing CXCR7, using anti-CXCR7 APC-antibody (R&D FAB4227A clone 11G8). The cells were counted through a FACS Canto II cytofluorometer (Becton Dickinson Immunocytometry Systems, Mountain View, CA, USA).

Migration Assay. Migration was assayed in 24-well Transwell chambers (Corning Inc., Corning, NY) using inserts with 5- and 8-μm (optimal for lymphocytes and epithelial cells, respectively) pore membranes. Membranes were pre-coated with collagen (human collagen type I/III) and fibronectin (20 μg/mL each). Cells were placed in the upper chamber (2×10^5cells/well) in culture medium containing 1% BSA (migration media) in the presence of the peptide; 100 ng/mL CXCL12 was added to the lower chamber. After 18 h incubation, cells atop the filter were removed using a cotton wool swab; migration of cells in the lone medium (control) was compared with that observed in media containing CXCL12. The cells were counted in ten different fields (original 400X magnification). The migration index was defined as the ratio between migrating cells in the experimental group and migrated cells in the control group.

Immunoblotting. Cells were homogenized in lysis buffer (40 mM Hepes pH 7.5, 120 mM NaCl, 5 mM $MgCl_2$, 1 mM EGTA, 0,5 mM EDTA, 1% Triton X-100) containing protease (Complete Tablets-EDTA free, Roche) and phosphatase inhibitors (20 mM a-glycerol-3-phosphate, 2.5 mM Na-pyrophosphate). The following primary antibodies were used: anti-P-ERK (sc7383, Santa Cruz Biotechnology, Inc., Santa Cruz, CA, USA) and anti-ERK2 (sc 154G, Santa Cruz Biotechnology

CA, USA). P-ERK induction was plotted as the ratio between P-ERK in the presence of CXCL12 (100 ng/ml) and P-ERK in free serum.

Receptor internalization assay. HCT-116-GFP-CXCR4 cell line was established in our lab by transfecting pEGFP-CXCR4 plasmid (Origene, USA) into the parental HCT-116 cell line; GFP-CXCR4 expression in selected HCT-116 clones was then confirmed by Flow cytometry and Immunofluorescence using anti-CXCR4 12G5 antibody (not shown). Subconfluent HCT-116-GFP-CXCR4 cells were grown on 10 mm coverslips in DMEM plus 10 % FBS-1 % P/S-1 % Glutammine for 1 day, washed with PBS plus 0.5 % BSA and equilibrated in DMEM plus 0.5 % BSA (Sigma-Aldrich). Cells were then exposed to **1** (0.1 μM) or **9** (0.1 μM) for 45 min at 37°C. Cells were then treated with 50 mg/ml CXCL12 and incubate at 37 °C for 45 min, fixed with 4% formaldehyde for 10 min, washed three times in PBS, permeabilized with 0.1% Triton X-PBS for 10 min and washed 3 times again in PBS. Cells were finally stained with α-tubulin/Alexa Fluor 594 and DAPI and inspected with a Zeiss LSM 510 confocal microscope equipped with Zeiss 2014 software.

NMR Spectroscopy and Computational Studies

The samples in micelle solution (200 mM of SDS-d_{25}) for NMR spectroscopy were prepared by dissolving the peptides in 0.18 mL of $^{1}H_2O$ (pH 5.5), 0.02 ml of $^{2}H_2O$ to obtain a concentration 2 mM of peptides. 2D DQF-COSY,[27] TOCSY,[28] and NOESY[29] spectra were recorded on a Varian INOVA 700 MHz spectrometer equipped with a z-gradient 5 mm triple-resonance probe head at a temperature of 298 K. The water signal was suppressed by gradient echo.[37] A mixing time of 80 ms and 200 ms was used for the TOCSY and NOESY experiments, respectively. The interactive program package XEASY[30] was used for the NMR analysis of DQF-COSY, TOCSY, and NOESY spectra. $^{3}J_{HN\text{-}H\alpha}$ coupling constants were acquired from 1D ^{1}H NMR and 2D DQF-COSY spectra.

The temperature coefficients of the amide proton chemical shifts were calculated from 1D ^{1}H NMR and 2D TOCSY experiments executed at different temperatures in the range 298 K – 313 K by means of linear regression.

Structural Determinations. The NOE cross peaks were integrated with the XEASY program and were converted into upper distance bounds using the CALIBA software provided by the program package DYANA.[38] Only NOE derived constraints (Table S3 and S4) were considered in the annealing procedures. An ensemble of 100 structures was generated with the simulated annealing calculations followed by successive steps of restrained and unrestrained energy minimization using the Discover algorithm (Accelrys, San Diego, CA). From the produced 100 conformations, 10 structures were chosen, whose inter-proton distances best fitted NOE derived distances.

Molecular modeling. A manual docking of the **9** averaged NMR structure in the crystal structure of CXCR4 in complex with the 16-mer cyclic peptide antagonist CVX15 (PDB code: 3OE0) was first accomplished. Specifically, we superimposed the coordinates of the Cα carbons of Arg^{4}, Phe^{5} and Phe^{6} in **9** with the Cα carbons of Arg^{1}, Arg^{2} and Nal^{3} in CVX15, which was then removed from the complex. Subsequently, to limit steric clash within the CXCR4 binding cavity, the side chains of Arg^{1} and Arg^{4} in **9** were manually extended to interact with Asp181 and Asp97, respectively. Prior to MD simulations, the receptor first N-terminal (K25) and the last C-terminal (A301) residues were capped with ACE and NME, respectively, while missing intracellular loops (ICL1 and ICL3) were added and refined using Prime.[39] Histidine tautomeric/protonation states were assigned through the PROPKA module of the Maestro Protein Preparation Wizard.[40] The refined complex was embedded in a POPC (1-Palmitoyl-2-oleoylphosphatidylcholine) phospholipids bilayer to mimic the physiological environment and then submitted to an over 100-ns MD simulation with NAMD 2.9.[41] In detail, a 94 Å × 94 Å (in x and y axes) pre-equilibrated

POPC phospholipid bilayer was firstly created with the aid of the membrane-builder tool of CHARMM-GUI.org (http://www. charmm-gui.org). With the purpose of placing the receptor into the bilayer, a hole was generated, and all lipids in close contact (<1 Å distance from any protein atoms) were deleted. The complex was then solvated using the solvation module of VMD 1.9.2, using the TIP3 water model. The *ff14SB* and *lipid14* Amber force fields[42] were used to parameterize the protein and the peptide, and the lipids, respectively. The addition of six Cl^- ions ensured neutrality. A 10 Å cutoff (switched at 8 Å) was used for atom pair interactions. The long-range electrostatic interactions were computed by means of the particle mesh Ewald (PME) method using a 1.0 Å grid spacing in periodic boundary conditions. The RATTLE algorithm was applied to constrain bonds involving hydrogen atoms; thus, a 2 fs integration time step interval could be used. The system was minimized and heated up to 300 K applying harmonic constraints, which were gradually released along the equilibration process. To prevent any distortion in the receptor secondary structural elements, these were constrained for further 10 ns. Production run was then performed in the NPT ensemble, at 1 atm and 300 K.

The same protocol was followed for the **1**/CXCR4 complex.

All of the pictures were rendered using PyMOL (www.pymol.org).

ASSOCIATED CONTENT

Supporting Information. Details of MD production runs; binding mode of **1** and its superposition with **9** at the CXCR4 binding site; NMR resonance assignments of **1** and **9** in SDS-$_{d25}$ solution at 298 K; NOE derived upper limit constraints of **1** and **9**.

AUTHOR INFORMATION

Corresponding Author

*For L.M.: phone, 0039-328-6795645; E-mail, lmarinel@unina.it

*For S.S.: phone, 0039-081-5903678, 0039-380-3140318; E-mail, s.scala@istitutotumori.na.it

Author Contributions

The manuscript was written through contributions of all authors. All authors have given approval to the final version of the manuscript. S.D.M. and A.M.T. equally contributed to this work.

Notes

The authors declare no competing financial interest.

ACKNOWLEDGMENTS

This research was funded by Scientific Independence of Young Researchers (SIR) 2014 (RBSI142AMA) to S.D.M.

ABBREVIATIONS

ACE, acetyl; CCL, CC chemokine ligand; CCR, CC chemokine receptor; CXCL, CC chemokine ligand; CXCR, CXC chemokine receptor; DCM, dichloromethane; DIEA, N,N-diisopropylethylamine; DMF, N,N-dimethylformamide; ECL, extracellular loop; GPCR, G protein-coupled receptor; HBTU, O-benzotriazole-N,N,N′,N′-tetramethyl-uroniumhexafluorophosphate; HOBt, N-hydroxybenzotriazole; IC, inhibitory concentration; MD, molecular dynamics; ICL, intracellular loop, NME, N-methyl; NMR, nuclear magnetic resonance; NOESY, nuclear Overhauser effect spectroscopy; POPC, 1-Palmitoyl-2-oleoylphosphatidylcholine; SAR, structure–activity relationship; SD, standard deviation; SDF-1α, stromal cell–derived factor–1; SDS, sodium dodecylsulphate; TIS, triisopropylsilane; TFA,

trifluoroacetic acid; TLC, thin layer chromatography; TOCSY, total correlation spectroscopy; VEGF, vascular endothelial growth factor.

REFERENCES

1. Blanchet, X.; Langer, M.; Weber, C.; Koenen, R. R.; and Von Hundelshausen, P. Touch of chemokines. *Front. Immunol.* **2012**, *3*, 175, 1–18.

2. Premack, B. A.; Schall, T. J. Chemokine receptors: gateways to inflammation and infection. *Nat. Med.* **1996**, *2*, 1174–1178.

3. Zlotnik, K.; Yoshie, O. Chemokines: a new classification system and their role in immunity. *Immunity* **2000**, *12*, 121–127.

4. Fernandez, E. J.; Lolis, E. Structure, Function, and Inhibition of Chemokines. *Annual Review of Pharmacology and Toxicology* **2002**, *42*, 469–499.

5. Scala, S. Molecular Pathways: Targeting the CXCR4-CXCL12 Axis--Untapped Potential in the Tumor Microenvironment. *Clin. Cancer Res*. **2015**, *21*, 4278–4285.

6. a) Feng, Y.; Broder, C. C.; Kennedy, P. E.; Berger, E. A. HIV-1 entry cofactor: functional cDNA cloning of a seven-transmembrane, G protein-coupled receptor. *Science* **1996**, *272*, 872–877. b) Vicenzi, E.; Liò, P.; Poli, G. The Puzzling Role of CXCR4 in Human Immunodeficiency Virus Infection *Theranostics* **2013**, *3*, 18–25. c) Demmer, O.; Frank, A. O.; Hagn, F.; Schottelius, M.; Marinelli, L.; Cosconati, S.; Brack-Werner, R.; Kremb, S.; Wester, H.J.; Kessler, H. A Conformationally Frozen Peptoid Boosts CXCR4 Affinity and Anti-HIV Activity. *Angew. Chem. Int. Ed*. **2012**, *51*, 8110–8113.

7. Yamada, M.; Kubo, H.; Kobayashi, S.; Ishizawa, K.; He, M.; Suzuki, T.; Fujino, N.; Kunishima, H.; Hatta, M.; Nishimaki, K.; Aoyagi, T.; Tokuda, K.; Kitagawa, M.; Yano, H.; Tamamura, H.; Fujii, N.; Kaku, M. The increase in surface CXCR4 expression on lung extravascular neutrophils and its effects on neutrophils during endotoxin-induced lung injury. *Cellular & Molecular Immunology* **2011**, *8*, 305–314.

8. a) Domanska, U. M.; Kruizinga, R. C.; Nagengast, W. B.; Timmer-Bosscha, H.; Huls, G.; de Vries, E. G.; Walenkamp, A. M. A review on CXCR4/CXCL12 axis in oncology: no place to hide. *Eur J Cancer*. **2013**, *49*, 219–230. b) Müller, A.; Homey, B.; Soto, H.; Ge, N.; Catron, D.; Buchanan, M. E.; Mcclanahan, T.; Murphy, E.; Yuan, W.; Wagner, S. M.; Barrera, J. L.; Mohar, A.; Vera´stegui, E.; Zlotnik, A. Involvement of chemokine receptors in breast cancer metastasis.

Nature **2001**, *410*, 50–56. c) Demmer, O.; Dijkgraaf, I.; Schumacher, U.; Marinelli, L.; Cosconati, S.; Gourni, E.; Wester, H. J.; Kessler, H. Design, synthesis, and functionalization of dimeric peptides targeting chemokine receptor CXCR4. *J. Med. Chem*. **2011**, *54,* 7648–62.

9. a) Burger, J. A.; Peled, A. CXCR4 antagonists: targeting the microenvironment in leukemia and other cancers. *Leukemia* **2009**, *23*, 43–52.

10. a) Ottaiano, A.; Franco, R.; Aiello Talamanca, A.; Liguori, G.; Tatangelo, F.; Delrio, P.; Nasti, G.; Barletta, E.; Facchini, G.; Daniele, B.; Di Blasi, A.; Napolitano, M.; Ieranò, C.; Calemma, R.; Leonardi, E.; Albino, V.; De Angelis, V.; Falanga, M.; Boccia, V.; Capuozzo, M.; Parisi, V.; Botti, G.; Castello, G.; Iaffaioli, R. V.; Scala, S. Overexpression of both CXC chemokine receptor 4 and vascular endothelial growth factor proteins predicts early distant relapse in stage II-III colorectal cancer patients. *Clin. Cancer Res.* **2006**, *12*, 2795–2803; b) D'Alterio, C.; Avallone, A.; Tatangelo, F.; Delrio, P.; Pecori, B.; Cella, L.; Pelella, A.; D'Armiento, F. P.; Carlomagno, C.; Bianco, F.; Silvestro, L.; Pacelli, R.; Napolitano, M.; Iaffaioli, R. V.; Scala, S. A prognostic model comprising pT stage, N status, and the chemokine receptors CXCR4 and CXCR7 powerfully predicts outcome in neoadjuvant resistant rectal cancer patients. *Int. J. Cancer* **2014**, *135*, 379–390; c) Ingold, B.; Schulz, S.; Budczies, J.; Neumann, U.; Ebert, MP.; Weichert, W.; Röcken, C. The role of vascular CXCR4 expression in colorectal carcinoma. *Histopathology* **2009**, *55*, 576–586; d) Wang, X.; Ding, X.; Nan, L.; Wang, Y.; Wang, J.; Yan, Z.; et al. Investigation of the roles of exosomes in colorectal cancer liver metastasis. *Oncol Rep.* **2015**, *33*, 2445–2453.

11. (a) Zlotnik, A. New insights on the role of CXCR4 in cancer metastasis. *J. Pathol*. **2008**, *215*, 211–213; (b). A. Fulton, M.; The chemokine receptors CXCR4 and CXCR3 in cancer. *Curr. Oncol. Rep*. **2009**, *11*, 125–131; (c). Teicher, B. A.; Fricker, S. P. CXCL12 (SDF-1)/CXCR4 Pathway in Cancer. *Clin. Cancer Res.* **2010**, *16*, 2927–2931; (d) Mukherjee, D.; Zhao, J.; The Role of chemokine receptor CXCR4 in breast cancer metastasis. *Am. J. Cancer Res*. **2013**, *3*, 46–57.

12. De Clercq, E. The bicyclam AMD3100 story. *Nature Reviews Drug Discovery* **2003**, *2,* 581–587.

13. (a) Vose, J. M.; Ho, A. D.; Coiffier, B.; Corradini, P.; Khouri, I.; Sureda, A.; Van Besieng K.; Dipersio, J. Advances in mobilization for the optimization of autologous stem cell transplantation. *Leuk. Lymphoma* **2009**, *50*, 1412–1421; (b) Dugan, M. J.; Maziarz, R. T.; Bensinger, W. I.; Nademanee, A.; Liesveld, J.; Badel, K.; Dehner, C.; Gibney, C.; Bridger, G.; Calandra, G. Safety and preliminary efficacy of plerixafor (Mozobil) in combination with

chemotherapy and G-CSF: an open-label, multicenter, exploratory trial in patients with multiple myeloma and non-Hodgkin's lymphoma undergoing stem cell mobilization. *Bone Marrow Transplant*. **2010**, *45*, 39–47.

14. (a) Hendrix, C. W.; Collier, A. C.; Lederman, M. M.; Schols, D.; Pollard, R. B.; Brown, S.; Jackson, J. B.; Coombs, R. W.; Glesby, M. J.; Flexner, C. W.; Bridger, G. J.; Badel, K.; MacFarland, R. T.; Henson, G. W.; Calandra, G. Safety, pharmacokinetics, and antiviral activity of AMD3100, a selective CXCR4 receptor inhibitor, in HIV-1 infection. *J. Acquir. Immune Defic. Syndr.* **2004**, *37*, 1253–1262; (b) Micallef, I. N.; Stiff, P. J.; DiPersio, J. F.; Maziarz, R. T.; McCarty, J. M.; Bridger, G.; Calandra, G. Successful Stem Cell Remobilization Using Plerixafor (Mozobil) Plus Granulocyte Colony-Stimulating Factor in Patients with Non-Hodgkin Lymphoma: Results from the Plerixafor NHL Phase 3 Study Rescue Protocol. *Biol. Blood Marrow Transplant.* **2009**, *15*, 1578-1586.

15. Stone, N. D.; Dunaway, S. B.; Flexner, C.; Tierney, C.; Calandra, G. B.; Becker, S.; Cao, Y. J.; Wiggins, I. P.; Conley, J.; MacFarland, R. T.; Park, J. G.; Lalama, C.; Snyder, S.; Kallungal, B.; Klingman, K. L.; Hendrix, C. W. Multiple-dose escalation study of the safety, pharmacokinetics, and biologic activity of oral AMD070, as a selective CXCR4 receptor inhibitor, in human subjects. *Antiomicrob. Agents Chemother*. **2007**, *51*, 2351–2358.

16. Peled, A.; Abraham, M.; Avivi, I.; Rowe, J. M.; Beider, K.; Wald, H.; Tiomkin, L.; Ribakovsky, L.; Riback, Y.; Ramati, Y.; Aviel, S.; Galun, E.; Shaw, H. L.; Eizenberg, O.; Hardan, I.; Shimoni, A.; Nagler, A. The high affinity CXCR4 antagonist BKT140 is safe and induces a robust mobilization of human CD34+ cells in patient with multiple myeloma. *Clin. Cancer Res.* **2014**, *20*, 469–479.

17. Kwong, J.; Kulbe, H.; Wong, D.; Chakravarty, P.; Balkwill, F. An antagonist of chemokine receptor CXCR4 induces mitotic catastrophe in ovarian cancer cell. *Mol. Cancer Ther*. **2009**, *8*, 1893–1905.

18**.** a) Peng, S. B.; Zhang, X.; Paul, D.; Kays, L. M.; Gough, W.; Stewart, J.; Uhlik, M. T.; Chen, Q.; Hui, Y. H.; Zamek-Gliszczynski, M. J.; Wijsman, J. A.; Credille, K. M.; Yan, L. Z. Identification of LY2510924, a novel cyclic peptide CXCR4 antagonist that exhibits antitumor activities in solid tumor and breast cancer metastatic models. *Mol. Cancer Ther.* **2015**, *14*, 480–490. b) Galsky, M. D.; Vogelzang, N. J.; Conkling, P.; Raddad, E.; Polzer, J.; Roberson, S.; Stille,

J. R.; Saleh, M.; Thornton, D. A phase I trial of LY2510924, a CXCR4 peptide antagonist, in patients with advanced cancer. *Clin. Cancer Res*. **2014**, *20*, 3581–3588.

19. Portella, L.; Vitale, R.; De Luca, S.; D'Alterio, C.; Ieranò, C.; Napolitano, N.; Riccio, A.; Polimeno, M. N.; Monfregola, L.; Barbieri, A.; Luciano, A.; Ciarmiello, A.; Arra, C.; Castello, G.; Amodeo, P.; Scala, S. Preclinical Development of a Novel Class of CXCR4 Antagonist Impairing Solid Tumors Growth and Metastases. *Plos One* **2013**, *8*, 1–9.

20. Fujii, N.; Oishi, S.; Hiramatsu, K.; Araki, T.; Ueda, S.; Tamamura, H.; Otaka, A.; Kusano, S.; Terakubo, S.; Nakashima, H.; Broach, J. A.; Trent, J. O.; Wang, Z.; Peiper, S. C. Molecular-size reduction of a potent CXCR4-chemokine antagonist using orthogonal combination of conformation- and sequence-based libraries. *Angew. Chem. Int. Ed.* **2003**, *42*, 3251–3253.

21. Siedler, F.; Weyher, E.; Moroder. L. Cysteine racemization in peptide synthesis: a new and easy detection method. *J. Pept. Sci*. **1996**, *2*, 271–275.

22. Fricker, S. P.; Anastassov, V.; Cox, J.; Darkes, M. C.; Grujic, O.; Idzan, S. R.; Labrecque, J.; Lau, G.; Mosi, R. M.; Nelson, K. L.; Qin, L.; Santucci, Z.; Wong R. S. Y. Characterization of the molecular pharmacology of AMD3100: a specific antagonist of the G-protein coupled chemokine receptor, CXCR4. *Biochem. Pharmacol.* **2006**, *72*, 588–596.

23. Kawada, K.; Hosogi, H.; Sonoshita, M.; Sakashita, H.; Manabe, T.; Shimahara, Y.; Sakai, Y.; Takabayashi, A.; Oshima, M.; Taketo, M. M. Chemokine receptor CXCR3 promotes colon cancer metastasis to lymph nodes. *Oncogene* **2007**, *26*, 4679–4688.

24. Ribas, R.; Ghazoui, Z.; Gao, Q.; Pancholi, S.; Rani, A.; Dunbier, A.; Dowsett, M.; Martin, L. A. Identification of chemokine receptors as potential modulators of endocrine resistance in oestrogen receptor-positive breast cancers. *Breast Cancer Res*. **2014**, *16,* 1–15.

25. Mansfeld, F. M.; Toth, I. Synthesis and Plasma Stability of Disulfide-Bridged Cyclic Endomorphin-1 Derivatives. *International Journal of Organic Chemistry* **2012**, *2*, 1–6.

26. Wüthrich, K. *NMR of Proteins and Nucleic Acids*; John Wiley & Sons, Inc: New York, **1986**.

27. a) Piantini, U.; Sorensen, O. W.; Ernst, R. R. Multiple Quantum Filters for Elucidating NMR Coupling Network. *J. Am. Chem. Soc.* **1982**, *104*, 6800–6801; b) Marion, D.; Wüthrich, K. Application of Phase Sensitive Two-Dimensional Correlated Spectroscopy (COSY) for Measurements of 1H-1H Spin-Spin Coupling Constants in Proteins. *Biochem. Biophys. Res. Commun*. **1983**, *113*, 967–974.

28. Braunschweiler, L.; Ernst, R. R. Coherence Transfer by Isotropic Mixing: Application to Proton Correlation Spectroscopy. *J. Magn. Reson*. **1983**, *53*, 521–528.

29. Jenner, J.; Meyer, B. H.; Bachman, P.; Ernst, R. R. Investigation of Exchange Processes by Two-Dimensional NMR Spectroscopy. *J. Chem. Phys.* **1979**, *71*, 4546–4553.

30. Bartels, C.; Xia, T.; Billeter, M.; Guentert, P.; Wu¨thrich, K. The Program XEASY for Computer-Supported NMR Spectral Analysis of Biological Macromolecules. *J. Biomol. NMR* **1995**, *6*, 1–10.

31. a) Moroder, L.; Romano, R.; Guba, W.; Mierke, D. F.; Kessler, H.; Delporte, C.; Winand, J.; Christophe, J. New evidence for a membrane bound pathway in hormone receptor binding. *Biochemistry* **1993**, *32*, 13551–13559; b) Sargent, D. F.; Schwyzer, R. Membrane lipid phase as catalyst for peptide-receptor interactions. *Proc. Natl. Acad. Sci.* U.S.A. **1986**, *83*, 5774–5778.

32. a) Di Cianni, A.; Carotenuto, A.; Brancaccio, D.; Novellino, E.; Reubi, J. C.; Beetschen, K.; Papini, A. M.; Ginanneschi, M. Novel octreotide dicarba-analogues with high affinity and different selectivity for somatostatin receptors. *J. Med. Chem*. **2010**, *53*, 6188–6197; b) Grieco, P.; Carotenuto, A.; Campiglia, P.; Gomez-Monterrey, I.; Auriemma, L.; Sala, M.; Marcozzi, C.; d'Emmanuele di Villa Bianca, R.; Brancaccio, D.; Rovero, P.; Santicioli, P.; Meini, S.; Maggi, C. A.; Novellino, E. New Insight into the Binding Mode of Peptide Ligands at Urotensin-II Receptor: Structure−Activity Relationships Study on P5U and Urantide. *J. Med. Chem*. **2009**, *52*, 3927−3940.

33. Thiele, S.; Mungalpara, J.; Steen, A.; Rosenkilde, M. M.; Våbenø, J. Determination of the binding mode for the cyclopentapeptide CXCR4 antagonist FC131 using a dual approach of ligand modifications and receptor mutagenesis. *Br. J. Pharmacol.* **2014**, *171*, 5313−5329.

34. Wu, B; Chien, E. Y.; Mol, C. D.; Fenalti, G.; Liu, W.; Katritch, V.; Abagyan, R.; Brooun, A.; Wells, P.; Bi, F. C.; Hamel, D. J.; Kuhn, P.; Handel, T. M.; Cherezov, V.; Stevens, R. C. Structures of the CXCR4 chemokine GPCR with small-molecule and cyclic peptide antagonists. *Science* **2010**, *330*, 1066−1071.

35. Kaiser, E.; Colescott, R. L.; Bossinger, C. D.; Cook, P. I. Color test for detection of free terminal amino groups in the solid-phase synthesis of peptides. *Anal. Biochem.* **1970**, *34*, 595−598.

36. Hancock, W. S.; Battersby, J. E. A new micro-test for the detection of incomplete coupling reactions in solid-phase peptide synthesis using 2,4,6-trinitrobenzenesulphonic acid. *Anal. Biochem.* **1976**, *71*, 260−264.

37. Hwang, T. L.; Shaka, A. J. Water suppression that works. Excitation sculpting using arbitrary wave-forms and pulsed-field gradients. *J. Magn. Reson.* **1995**, *112*, 275–279.

38. Güntert, P.; Mumenthaler, C.; Wüthrich, K. Torsion Angle Dynamics for NMR Structure Calculation with the New Program DYANA. *J. Mol. Biol.* **1997**, *273*, 283–298.

39. Prime, version 4.0, Schrödinger, LLC, New York, NY, **2015**.

40. Maestro, version 10.1; Schrödinger, LLC: New York, **2009**.

41. Phillips, J. C.; Braun, R.; Wang, W.; Gumbart, J.; Tajkhorshid, E.; Villa, E.; Chipot, C.; Skeel, R. D.; Kale, L.; Schulten, K. Scalable molecular dynamics with NAMD. *J. Comput. Chem.* **2005**, *26*, 1781–1802.

42. Case, D. A.; Babin, V.; Berryman, J. T.; Betz, R. M.; Cai, Q.; Cerutti, D. S.; Cheatham III, T. E.; Darden, T. A.; Duke, R. E.; Gohlke, H.; Goetz, A.W.; Gusarov, S.; Homeyer, N.; Janowski, P.; Kaus, J.; Kolossvary, I.; Kovalenko, A.; Lee, T. S.; LeGrand, S.; Luchko, T.; Luo, R.; Madej, B.; Merz, K. M.; Paesani, F.; Roe, D. R.; Roitberg, A.; Sagui, C.; Salomon-Ferrer, R.; Seabra, G.; Simmerling, C. L.; Smith, W. L.; Swails, J.; Walker, R. C.; Wang, J.; Wolf, R. M.; Wu, X.; Kollman, P. A. AMBER 14 *Reference Manual*, **2014**, pp. 29–31.

Table of Contents graphic